

NUMERICALLY SIMULATING CARBONATE MINERALIZATION OF BASALT WITH INJECTION OF CARBON DIOXIDE INTO DEEP SALINE FORMATIONS

M. D. WHITE¹, B. P. MCGRAIL², H. T. SCHAEF², AND D. H. BACON¹

¹ *Hydrology Group, Pacific Northwest National Laboratory, P.O. Box 999, Richland, WA, 99352, United States, mark.white@pnl.gov, diana.bacon@pnl.gov*

² *Applied Geology and Geochemistry, Pacific Northwest National Laboratory, P.O. Box 999, Richland, WA, 99352, United States, pete.mcgrail@pnl.gov, todd.schaeff@pnl.gov*

ABSTRACT

The principal mechanisms for the geologic sequestration of carbon dioxide in deep saline formations include geological structural trapping, hydrological entrapment of nonwetting fluids, aqueous phase dissolution and ionization, and geochemical sorption and mineralization. In sedimentary saline formations the dominant mechanisms are structural and dissolution trapping, with moderate to weak contributions from hydrological and geochemical trapping; where, hydrological trapping occurs during the imbibition of aqueous solution into pore spaces occupied by gaseous carbon dioxide, and geochemical trapping is controlled by generally slow reaction kinetics. In addition to being globally abundant and vast, deep basaltic lava formations offer mineralization kinetics that make geochemical trapping a dominate mechanism for trapping carbon dioxide in these formations. For several decades the United States Department of Energy has been investigating Columbia River basalt in the Pacific Northwest as part of its environmental programs and options for natural gas storage. Recently this nonpotable and extensively characterized basalt formation is being reconsidered as a potential reservoir for geologic sequestration of carbon dioxide. The reservoir has an estimated storage capacity of 100 giga tonnes of carbon dioxide and comprises layered basalt flows with sublayering that generally alternates between low permeability massive and high permeability breccia. Chemical analysis of the formation shows 10 wt% Fe, primarily in the +2 valence. The mineralization reaction that makes basalt formations attractive for carbon dioxide sequestration is that of calcium, magnesium, and iron silicates reacting with dissolved carbon dioxide, producing carbonate minerals and amorphous quartz. Preliminary estimates of the kinetics of the silicate-to-carbonate reactions have been determined experimentally and this research is continuing to determine affects of temperature, pressure, rock composition and mineral assemblages on the reaction rates. This study numerically investigates the injection, migration and sequestration of supercritical carbon dioxide in deep Columbia River basalt formations using the multifluid subsurface flow and reactive transport simulator STOMP-CO2 with its ECKEChem module. Simulations are executed on high resolution multiple stochastic realizations of the layered basalt systems and demonstrate the migration behavior through layered basalt formations and the mineralization of dissolved carbon dioxide. Reported results include images of the migration behavior, distribution of carbonate formation, quantities of injected and sequestered carbon dioxide, and percentages of the carbon dioxide sequestered by different mechanisms over time.

1. INTRODUCTION

Geologic sequestration of anthropogenic carbon dioxide (CO_2) in deep saline formations in sedimentary rock is being practiced commercially by Statoil off the shores of Norway at the Sleipner facility. The main advantages of saline formations in sedimentary rocks for geologic sequestration are their large potential storage volume and common occurrence globally. For sedimentary rock reservoirs the sequestration mechanisms during the prograde (active injection) period are hydraulic trapping and dissolution trapping. During the retrograde (post injection) period hydrodynamic trapping, via hysteretic gas entrapment, becomes possible as saline water displaces supercritical CO_2 . For longer time scales mineralization trapping, through the acid dissolution of formation minerals and precipitation of carbonates additionally contributes to the trapping mechanisms (Johnson et al. 2001).

Another type of saline formation that has the potential for sequestering CO_2 is basalt. Because basalt rock is dense and impermeable, it would seem to be an unlikely candidate for CO_2 sequestration. However, basalt formations are layered structures formed from periodic lava flows; where the faster-cooling flow tops are highly fractured and rubbled and permeable, and the underlying slower-cooling flow interiors are dense and impermeable. Therefore the target horizons for CO_2 injection and sequestration in basalt formation are the permeable fractured and rubbled flow tops.

Although multilayered basalts are not as ubiquitous as deep sedimentary rock saline formations, major basalt formations occur in the northwest, southeast, and northern Midwest regions of the United States. Worldwide, basalt formations occur across the enormous Deccan Plateau, encompassing most of central and southern India, and in vast tracts of Siberia. The Columbia River Basalt Group, located in northwestern United States, comprises 220,000 km^3 with preliminary estimates of storage capacity being 90 billion ktonnes. Fractured and rubbled basalt layers lack the pore morphology that induces hysteretic trapping of nonwetting fluid phases, such as supercritical CO_2 in a saline formation; however, the other trapping mechanisms for saline formations are active (i.e., hydraulic, dissolution, and mineralization). It is the high permeability and mineralization trapping mechanism that makes basalt formations most attractive for sequestering CO_2 . Preliminary kinetics testing using basalts from the Columbia River Basalt Group, the Southeast Rift Zone, the Newark Supergroup within the United States, the Deccan formations in western India and the Karoo formations in southern Africa are showing rapid dissolution rates for the basalt at a pH of 4.0 and similarly rapid precipitation rates of calcite under supercritical CO_2 conditions.

To investigate the sequestration of CO_2 in deep saline basalt formations a series of numerical simulations were conducted on a two-dimensional representation of an injection well within the Columbia River Basalt Group. The numerical simulations were conducted with STOMP- CO_2 with its new ECKEChem (Equilibrium-Conservation-Kinetic Chemistry) reactive transport module (White and McGrail 2005). The simulations considered the following important factors affecting the injection and sequestration of CO_2 in saline basalt formations: 1) injectivity of the basalt formation using a stochastically generated realization of the formation using four basalt classifications based on physical characteristics (breccia, massive, vesicular, and vuggy), 2) CO_2 solubility depending on the temperature, pressure, and salinity, 3) dissolution of basalt with the injection of CO_2 and subsequent precipitation of carbonates, and 4) alteration of the basalt intrinsic permeability and porosity with basalt dissolution and carbonate precipitation. Relative and absolute quantities of sequestered CO_2

are reported for the three principal sequestration mechanisms for basalts: 1) hydraulic trapping, 2) dissolution trapping, and 3) mineral trapping.

2. NUMERICAL APPROACH

The reported simulation results were generated by STOMP-CO₂ (White and Oostrom, 2000) with its new chemistry module ECKEChem (White and McGrail, 2005). STOMP-CO₂ is an isothermal multifluid flow simulator that solves nonlinear conservation equations for water mass, CO₂ mass, and salt mass, with transport occurring over two mobile phases; aqueous and gas. The equation-of-state module considers liquid, gaseous and supercritical conditions for CO₂ using the formulations of Span and Wagner (1996), but the multifluid system does not allow for liquid CO₂ as a separate phase. The governing equations are discretized spatially on structured orthogonal grids, using the integral finite difference approach and temporally using first-order backward Euler differencing, yielding a fully implicit system of nonlinear equations. The nonlinearities that arise through the constitutive equations that relate the primary and secondary variables are resolved using Newton-Raphson iteration, applying a primary variable switching scheme for phase transitions. The multifluid flow equations are coupled to the reactive transport equations through a noniterative sequential approach, and the reactive transport equations are solved using an operator splitting approach; where the transport and chemical reactions are solved separately. To minimize the number of transported species only mobile conservation- and kinetic-component species are transported. The multifluid flow and reactive transport equations are linked through the total aqueous CO₂, dissolved basalt, and precipitated carbonates. Total aqueous CO₂ concentrations for the chemical reaction solution are obtained from the multifluid flow solution and the resulting change in total aqueous CO₂ concentration through carbonate precipitation or dissolution reactions is coupled back to the multifluid flow equations as CO₂ mass sources. Changes in the primary and secondary mineral concentrations are used to alter the porosity and intrinsic permeability of the formation, which then affect the multifluid flow system. As a noniterative sequential approach is used to couple the multifluid flow and reactive transport solutions, changes in CO₂ mass, porosity, and intrinsic permeability are time lagged.

2.1 ECKEChem Overview.

Chemical reactions can be classified as being either sufficiently fast enough to be reversible or in equilibrium or insufficiently fast enough for equilibrium conditions to apply, requiring a kinetic description. Geochemical reactive systems that occur in subsurface environments generally require both equilibrium and kinetic reaction types to describe the system. The ECKEChem (Equilibrium-Conservation-Kinetic-Equation Chemistry) solver module for the STOMP simulator uses a reaction-based model (Fang et al., 2003) for the chemical system; where reactions are assumed to be fast/equilibrium or slow/kinetic. Equilibrium reactions are modeled using an infinite reaction rate via equilibrium equations, and kinetic reactions have finite reaction rates and are modeled using kinetic equations. To complete the chemical reaction system conservation equations are generated. The ECKEChem solver assumes that the geochemical system can be completely described through

equilibrium, conservation, and kinetic equations. To translate a geochemical reaction network into an ECKE system a formal decomposition approach has been adopted (Fang et al., 2003). This decomposition approach has been coded into a preprocessor that allows rapid translation of a complex geochemical reaction network into an ECKE system.

A complete ECKE system involves a set of equilibrium, conservation, and kinetic equations equal in number to the number of unknown species concentrations. The resulting system of equations is nonlinear and is solved using Newton-Raphson iteration. Equilibrium equations, often referred to as mass action equilibrium equations relate species activities through a equilibrium constant:

$$(C_j) = K_{eq\ j} \prod_{N_{eq\ j}^s} (C_i)^{e_i} (i \neq j); \text{ for } j = 1, N_{eq}^{eq} \quad (1)$$

where the exponents are stoichiometric coefficients in the reaction network and the equilibrium constant can be temperature dependent. Conservation equations define the component species, which essentially are a set of species, whose collective stoichiometrically weighted summed concentration is invariant with time:

$$\frac{d \sum_{N_{ic\ j}^s} (a_i C_i)}{dt} = 0; \text{ for } j = 1, N_{cn}^{eq} \quad (2)$$

Kinetic equations define kinetic components and are similar in form to conservation equations, except that stoichiometrically weighted sum of species concentrations vary in time according to a weighted sum of kinetic rates:

$$\frac{d \sum_{N_{ik\ j}^s} (b_i C_i)}{dt} = \sum_{N_{tk\ j}^r} (c_k R_k); \text{ for } j = 1, N_{kn}^{eq} \quad (3)$$

2.2 Hydrologic conceptual model.

The hydrologic conceptual model for the numerical simulations of CO₂ sequestration in basalt was developed from data collected from a single borehole (designated DC-6 (699-54-18)), drilled in 1977-1978, on the Hanford Site, near Richland, Washington, United States, which is within the Columbia River Basalt Group (CRBG). The borehole is cased to 689 m bgs, with an open corehole diameter of 7.7 cm to a depth of 1322 m bgs (Crowley and Ledgerwood, 1988). The computational domain is two-dimensional cylindrical system (100 x 500 nodes), centered on the borehole, which begins at 1158.6 m bgs and extends vertically 500 m, using a 1.0-m uniform grid spacing, and extends radially 8184.7 m, using log-linearly expanding grid spacing, with an inner radius congruent with the borehole. CO₂ was injected into the basalt, through the open borehole, over the lower 60-m, a region which was identified as having 70% of the entire borehole transmissivity. Isothermal conditions were assumed with a temperature of 50 °C in accordance to borehole data (Gephart, 1981). Realizations of the hydrologic properties of the basalt formation were generated with the sequential indicator simulation program SISIM from GSLIB (Deutsch and Journel, 1992), using four categories of basalt delineated from the interpretation of the borehole: 1) breccia, 2) massive, 3) vesicular, and 4) vuggy. Correlation lengths for the indicator simulation were derived from the borehole data. Hydrologic properties for the basalt categories are listed in TABLE 1, where θ is the porosity,

K_{sat} is the hydraulic conductivity, and ψ , λ , and s_{lr} , are Brooks and Corey (1964) soil moisture retention function parameters. Fluid-phase relative permeabilities were computed using the Mualem pore-size distribution model (1976). At the inner radial boundary (i.e., the borehole radius) the CO₂ injection pressure was 15.82 MPa, with a borehole pressure gradient of 0.136 MPa/m (6.0 psi/ft) borehole pressure gradient. The outer radial boundary was maintained at the initial pressure of 11.89 MPa, with a hydrostatic pressure gradient of 0.102 MPa/m (4.5 psi/ft).

TABLE 1. Basalt hydrologic properties

Basalt	θ	K_{sat}	ψ	λ	s_{lr}
Breccia	0.08	1.e-6 m/s	0.54 m	4.0	0.577
Massive	0.05	1.e-11 m/s	1.54 m	4.0	0.577
Vesicular	0.065	1.e-7 m/s	0.84 m	4.0	0.577
Vuggy	0.07	2.e-7 m/s	0.74 m	4.0	0.577

2.3 Basalt chemistry.

The CRBG formation is a typical example of a within-plate continental flood basalt (Caprarelli and Reidel, 2004). Its estimated volume is 220,000 km³ and was formed from over 300 lava flows, erupted from fissures, that occurred between 17.5 and 6 Ma. The basalt is composed almost entirely of tholeiitic lava and contains, in order of abundance, plagioclase feldspar, augite, pigeonite and a non-crystalline glassy mesostasis. Titaniferous magnetite and ilmenite grains are scattered throughout the rock. Flow tops are dominated by the glassy mesostasis. Supercritical CO₂ testing with crushed CRBG basalt show the conversion of CO₂ into a stable carbonate mineral occurs in a matter of days (McGrail et al., in review). Chemical compositions determined by x-ray fluorescence for a Columbia River Basalt sample are provided in TABLE 2. Based on this composition, the molecular weight of the basalt is calculated as 107.28 g/mol. The density of the basalt is 2.31 g cm⁻³.

TABLE 2. Composition of Columbia River Basalt.

Oxide	Weight %	Oxide	Weight %	Oxide	Weight %
SiO ₂	51.37	TiO ₂	2.11	BaO	0.05
Al ₂ O ₃	15.03	P ₂ O ₅	0.46	SrO	0.04
Fe ₂ O ₃	13.3	K ₂ O	0.44	ZnO	0.02
CaO	8.84	MnO	0.17	ZrO ₂	0.02
MgO	5.16	SO ₃	0.11	Cl ⁻	0.01
Na ₂ O	2.79	V ₂ O ₅	0.05		

Dissolution kinetics of the Columbia River Basalt were measured for a range of temperatures (25 to 90°C) under mildly acidic to neutral pH conditions using the single-pass flow-through test method (Schaefer and McGrail, in preparation). A non-linear regression was conducted using the data set collected at 40, 70, and 90°C following the kinetic rate law

$$R_k = k_o A_m 10^{\eta pH} \exp\left(\frac{E_a}{RT}\right) \quad (4)$$

where R_k is the release rate ($\text{mol}_{\text{basalt}} \text{s}^{-1}$), k_o is the intrinsic rate constant ($\text{mol}_{\text{basalt}} \text{m}^{-2} \text{s}^{-1}$), A_m is the specific mineral surface area ($\text{m}^2 \text{g}_{\text{basalt}}^{-1}$), η is the pH power law coefficient, E_a is the activation energy (J mol^{-1}), R is the ideal gas constant ($\text{J mol}^{-1} \text{K}^{-1}$), and T is the temperature (K). Under anaerobic conditions, the normalized dissolution rates for CRBG basalt decrease with increasing pH ($3 \leq \text{pH} \leq 7$) with a slope, η , of 0.12 ± 0.02 . An activation energy, E_a , has been estimated at $30.3 \pm 2.4 \times 10^3 \text{ J mol}^{-1}$. The intrinsic rate constant k_o was estimated to be $2.16 \pm 1.83 \times 10^{-3} \text{ mol}_{\text{basalt}} \text{m}^{-2} \text{s}^{-1}$. Dissolution kinetics measurements like these are essential data needed to model the rate at which the CO_2 reacts with basalt and would be converted to carbonate minerals in situ. A surface area of $2.5 \text{ m}^2 \text{g}^{-1}$ for the Columbia River Basalt was inferred based on measurements of another basalt (Kahle et al., 2004).

2.4 Chemical conceptual model.

Based on the composition of CRBG basalt and the groundwater hydrochemistry for the Cohasset flow bottom (822 m bgs), a candidate zone for CO_2 injection (unpublished data, 1988), dissolution of CRBG basalt in groundwater was simulated using EQ3/6 (Wolery and Jarek, 2003). A set of thermodynamically favorable secondary minerals was identified, after eliminating known high-temperature minerals. Equilibrium constants for the precipitation of each mineral were estimated at a temperature of 50°C based on data from the EQ3/6 database. Kinetic rate parameters for secondary minerals considered in simulations (Xu et al., 2004) are shown in TABLE 3. Kinetically controlled dissolution and precipitation of the secondary minerals used a “transition-state-theory” rate (Lasaga, 1982, Aagaard and Helgeson, 1983)

$$R_k = k_{25} A_m \exp\left[\frac{-E_a}{R} \left(\frac{1}{T} - \frac{1}{298.15}\right)\right] \left[\frac{Q_m}{K_m} - 1\right] \quad (5)$$

where R_k is the dissolution/precipitation rate ($\text{mol}_{\text{min}} \text{s}^{-1}$), + values indicate precipitation, k_{25} is rate constant at 25°C ($\text{mol}_{\text{min}} \text{m}^{-2} \text{s}^{-1}$), A_m is the specific mineral surface area ($\text{m}^2 \text{g}_{\text{min}}^{-1}$), E_a is the activation energy (J mol^{-1}), R is the ideal gas constant ($\text{J mol}^{-1} \text{K}^{-1}$), and T is the temperature (K). Equilibrium constants for both the equilibrium and kinetic reactions are shown in TABLE 4.

TABLE 3. Kinetic rate parameters for secondary minerals

Mineral	k_{25} ($\text{mol m}^{-2} \text{s}^{-1}$)	E_a (kJ mol^{-1})	Reference	A_m ($\text{m}^2 \text{g}^{-1}$)	Reference
calcite	1.6×10^{-9}	41.87	(Svensson and Dreybrodt, 1992)	2.0	(Vdovic, 2001)
chalcedony	1.0×10^{-13}	62.76	Set to kaolinite	2.0	(Leamson et al., 1969)
illite	1.0×10^{-14}	58.62	(Knauss and Worley, 1989)	33.8	(Hradil and Hostomsky, 2002)
kaolinite	1.0×10^{-13}	62.76	(Nagy, 1995)	23.5	(Hradil and Hostomsky, 2002)
magnesite	0.60×10^{-9}	41.87	based on calcite	2.0	set to calcite
nontronite-Ca	1.0×10^{-14}	58.62	set to illite	33.8	set to illite
nontronite-Mg	1.0×10^{-14}	58.62	set to illite	33.8	set to illite

TABLE 4. Equilibrium constants for equilibrium and kinetic reactions

Reaction	Log K_{eq}	Reaction	Log K_{eq}
$Al(OH)_2^+ = 2H^+ + AlO_2^-$	-11.198	$CO_2(aq) = H^+ + HCO_3^-$	-6.266
$CO_3^{2-} + H^+ = HCO_3^-$	10.167	$CaCO_3(aq) + H^+ = Ca^{2+} + HCO_3^-$	6.594
$CaCl^+ = Ca^{2+} + Cl^-$	0.632	$CaHCO_3^+ = Ca^{2+} + HCO_3^-$	-1.111
$CaOH^+ + H^+ = Ca^{2+}$	12.850	$H_2SiO_4^{-2} + 2H^+ = SiO_2(aq)$	22.960
$HAlO_2(aq) = H^+ + AlO_2^-$	-5.991	$HCl(aq) = Cl^- + H^+$	0.687
$HSiO_3^- + H^+ = SiO_2(aq)$	9.598	$KCl(aq) = Cl^- + K^+$	1.293
$MgCO_3(aq) + H^+ = HCO_3^- + Mg^{2+}$	7.035	$MgCl^+ = Cl^- + Mg^{2+}$	0.096
$MgHCO_3^+ = HCO_3^- + Mg^{2+}$	-1.111	$NaAlO_2(aq) = Na^+ + AlO_2^-$	0.592
$NaCO_3^- + H^+ = HCO_3^- + Na^+$	9.973	$NaCl(aq) = Cl^- + Na^+$	0.692
$NaHCO_3(aq) = HCO_3^- + Na^+$	0.037	$NaHSiO_3(aq) + H^+ = Na^+ + SiO_2(aq)$	8.128
$Calcite + H^+ = Ca^{2+} + HCO_3^-$	1.3909	$Chalcedony = SiO_2(aq)$	-3.3434
$Kaolinite = 2H^+ + 2SiO_2(aq) + 2AlO_2^-$	4.1707	$Magnesite + H^+ = HCO_3^- + Mg^{2+}$	1.5306
Reaction		Log K_{eq}	
$Illite = 1.2H^+ + 0.25Mg^{2+} + 0.6K^+ + 3.5SiO_2(aq) + 2.3AlO_2^-$		5.5551	
$Nontronite-Ca = 0.165Ca^{2+} + 3.670SiO_2(aq) + 0.330AlO_2^- + 2Fe(OH)_3(aq)$		-12.6234	
$Nontronite-Mg = 0.165Mg^{2+} + 3.670SiO_2(aq) + 0.330AlO_2^- + 2Fe(OH)_3(aq)$		-12.7160	
$Nontronite-Na = 0.330Na^+ + 3.670SiO_2(aq) + 0.330AlO_2^- + 2Fe(OH)_3(aq)$		-12.4420	
$Basalt + 0.394H^+ + 0.316AlO_2^- + 0.169Ca^{2+} + 0.179Fe(OH)_3(aq) + 0.01K^+ + 0.137Mg^{2+} + 0.097Na^+ + 0.917SiO_2(aq) + 0.0003Cl^-$		-7.2245	

3. RESULTS

Page restrictions prohibit the publication of the complete hydrological and geochemical numerical simulation results. These results will be presented during the oral presentation associated with this conference publication. As an indication of the CO₂ injection process without considering the impacts of geochemical dissolution and precipitation on the formation hydrologic properties, the mid-field CO₂ saturation profiles are shown in Figure 2, after

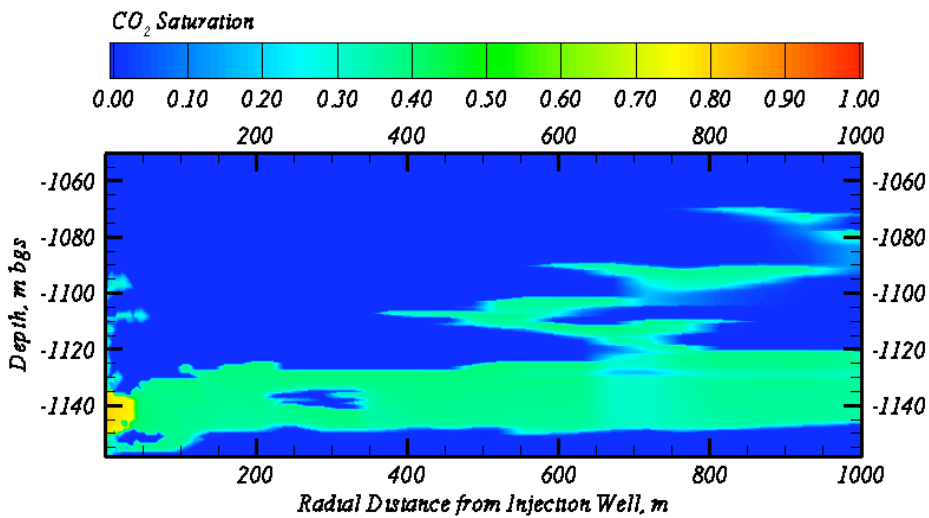


Figure 2. CO₂ Saturation Profiles after Injecting 17.5 years.

injecting CO₂ under constant borehole pressures for 17.5 years. The profile clearly shows the high lateral permeabilities associated with the rubble flow tops, with vertical migrations occurring between flow layers, where breaches occur in the massive basalt sub-layers.

REFERENCES

- Aagaard, P., and H. C. Helgeson (1983), Thermodynamic and kinetic constraints on reaction rates among minerals and aqueous solution. I. Theoretical considerations. *American Journal of Science*, 282, 237-285.
- Brooks, R. H., and A. T. Corey (1964), Hydraulic Properties of Porous Media. Colorado State University, Hydrology Paper, No. 3, Fort Collins, Colorado.
- Caprarelli, G. and S. P. Reidel (2004), Physical evolution of Grande Ronde Basalt magmas, Columbia River Basalt Group, north-western USA, *Mineralogy and Petrology* 80(1-2), 1-25.
- Crowley, W. H. and R. K. Ledgerwood (1988), Borehole Status Chart and Location Maps, Westinghouse Hanford Company, *SD-BWI-DP-044, Rev. 0*, Richland, Washington.
- Deutsch, C. V., and A. G. Journel (1997), *GSLIB: Geostatistical Software Library and User's Guide*. Oxford University Press, New York, 2nd Edition.
- Fang, Y., G.-T. Yeh, and W. D. Burgos (2003), A general paradigm to model reaction-based biogeochemical processes in batch systems, *Water Resources Research*, 39(4), 1083-1107.
- Gephart, R. E. (1981), Borehole DC-6: Hydrostratigraphic Chart, Rockwell Hanford Operations, *RHO-BWI-TI-063*, Richland, Washington.
- Johnson, J. W., J. J. Nitao, C. I. Steefel, and K. G. Knauss (2001), Reactive transport modeling of geologic CO₂ sequestration in saline formations: the influence of intra-aquifer shales and the relative effectiveness of structural, solubility, and mineral trapping during prograde and retrograde sequestration, In Proceedings of First National Conference on Carbon Sequestration, Washington, D.C., NETL.
- Hradil, D. and J. Hostomsky (2002), Effect of composition and physical properties of natural kaolinitic clays on their strong acid weathering rates, *Catena* 49, 171-181.
- Kahle, A., B. Winkler, A. Radulescu and J. Schreuer (2004), Small-angle neutron scattering study of volcanic rocks, *European Journal of Mineralogy* 16(3), 407-417.
- Lasaga, A. C. (1982), Transition state theory, in *Kinetics of Geochemical Process, Review of Mineralogy*, 8, edited by A. C. Lasaga and R. J. Kirkpatrick, pp. 169-195, Mineralogy Society of America.
- Leamson, R. N., J. Thomas, Jr. and H. P. Ehrlinger, III (1969), A study of the surface areas of particulate microcrystalline silica and silica sand, Illinois State Geological Survey Circular, 444.
- Mualem, Y. (1976), A new model for predicting the hydraulic conductivity of unsaturated porous media. *Water Resources Research*, 12, 513-522.
- Nagy, K. L. (1995), Dissolution and precipitation kinetics of sheet silicates, *Chemical Weathering Rates Silicate Minerals* 31, 291-351.
- Schaeff, H. T. and B. P. McGrail (in preparation), Dissolution of Columbia River Basalt under mildly acidic conditions relevant to geological sequestration of carbon dioxide, Pacific Northwest National Laboratory, Richland, Washington.
- Svensson, U. and W. Dreybrodt (1992), Dissolution kinetics of natural calcite minerals in CO₂-water systems approaching calcite equilibrium, *Chemical Geology* 100, 129-145.
- Vdovic, N. (2001), Electrokinetic behaviour of calcite—the relationship with other calcite properties, *Chemical Geology* 177, 241-248.
- Span, R., and W. Wagner (1996), A new equation of state for carbon dioxide covering the fluid region from the triple-point temperature to 1100 K at pressures up to 800 MPa, *J. Phys. Chem. Ref. Data*, 25(6), 1509-1596.
- White, M. D., and M. Oostrom (2000), STOMP Subsurface Transport Over Multiple Phases, Version 2.0, Theory Guide. Pacific Northwest National Laboratory, *PNNL-12030, UC-2010*, Richland, Washington.
- White, M. D., B. P. McGrail (2005), STOMP Subsurface Transport Over Multiple Phases, Version 1.0, Addendum: ECKEChem Equilibrium-Conservation-Kinetic Equation Chemistry and Reactive Transport, *PNNL-15482*, Pacific Northwest National Laboratory, Richland, Washington.
- Wolery, T. W. and R. L. Jarek (2003), Software User's Manual, EQ3/6, Version 8.0, *10813-UM-8.0-00*, Sandia National Laboratories, Albuquerque, New Mexico.
- Xu, T., J. A. Apps and K. Pruess (2004), Numerical simulation of CO₂ disposal by mineral trapping in deep aquifers, *Applied Geochemistry* 19, 917-936.